Dalton Transactions

Accepted Manuscript

ROYAL SOCIETY OF CHEMISTRY

www.rsc.org/dalton

Graphical abstract

La_2O_3-encapsulated-SnO_2 nanocrystallite-based photoanodes for enhanced DSSCs performance

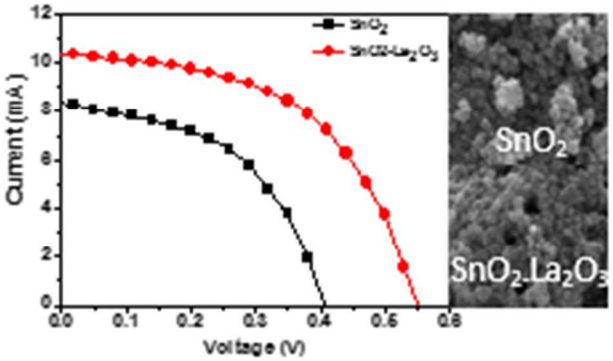

Cite this: DOI: 10.1039/c0xx00000x

www.rsc.org/xxxxxx

ARTICLE TYPE

La_2O_3-encapsulated SnO_2 nanocrystallite-based photoanodes for enhanced DSSCs performance

Shoyebmohamad F. Shaikh,[a,b] Rajaram S. Mane[a], and Oh-Shim Joo*[a]

Received (in XXX, XXX) Xth XXXXXXXXX 20XX, Accepted Xth XXXXXXXXX 20XX

DOI: 10.1039/b000000x

SnO_2 nanocrystallite-based photoanode was prepared by using tin (IV) chloride and fructose through one-pot hydrothermal method and attempted for its structural and morphological studies. Structural observation reveals tetragonal crystals of SnO_2 and morphological study has confirmed spherical nanoparticulates. Furthermore, surface of encapsulated SnO_2 photoanode (+N719 dye) with thin layers of La_2O_3 has significantly improved the short-circuit current density, open-circuit voltage, fill factor and power conversion efficiency values from 8.30 to 10.35 mA.cm^{-2}, 0.40 to 0.55 V, 49% to 55% and 1.66% to 3.00%, respectively. Nearly two-fold improvement in an energy conversion efficiency was attributed to; a) increased dye molecules caused by formation of strong co-ordination bonding between the dye molecules and lanthanide, b) enhanced photoelectron transfer rate between the dye molecules and SnO_2 conduction band, and c) negative shift of SnO_2 conduction band position in the presence of La_2O_3 (confirmed from the Mott-Schottky analysis).

1. Introduction

Dye-sensitized solar cells (DSSCs) have garnered considerable attention within the solar cell community due to their low-cost, chemical stability, ease of fabrication, and efficient solar-to-electricity conversion device, etc.[1,2] To date, semiconductors of mid band gap energies (2.8 – 3.8 eV) are promising photoanode materials for DSSCs application.[3] The nanoporous nature of photoanode materials provides large surface area for efficient dye adsorption, which delivers higher light harvesting and energy conversion efficiencies.[4] However, electron recombination occurred in electron transport processes, those of electron injection from excited dye to conduction band and electron transport from conduction band to conductive and transparent fluorine-tin-oxide (FTO) substrate of photoanode. In addition, reverse flow of electrons towards oxidized dye/reduced electrolyte, is considered as one of the major hurdles to achieve a high solar-to-electricity conversion efficiency.[5]

In DSSCs, photoanodes of a wide band gap metal oxide play two important roles such as an accumulation of dye molecules and transporter for injected photoelectrons. As a wide band gap metal oxide, TiO_2 is found to exhibit the highest power conversion efficiency owing to its specific optoelectronic properties.[6,7] On the other hand, low electron mobility in TiO_2 is the possible reason of high electron recombination rate which eventually opposes further improvement of power conversion efficiency.[8] Besides TiO_2, several studies have reported the merits and demerits of other metal oxides including ZnO, SnO_2, WO_3, and Nb_2O_5 etc., in DSSCs.[9-12] Among these semiconducting metal oxides, SnO_2 is an *n*-type semiconductor with many advantageous features compared to TiO_2 such as; a) electron mobility in SnO_2 (~100–250 cm^2 V-1 s^{-1}) is above two-orders of magnitude higher than TiO_2 (~0.1–1.0 cm^2 V^{-1} s^{-1}),[13] suggesting a faster diffusion transport of photo-induced electrons, b) has a lower band gap (3.4 eV) than anatase TiO_2 (3.2 eV), which would create fewer oxidative holes in the valence band (the fewer oxidative holes facilitate long-term stability, less dye-degradation rate and high stability under long-term UV radiation), and c) can easily form anisotropic structures, such as nanorods, nanowires and nanoflowers; capable to exhibit unique electronic and optical properties.[14] However, a DSSCs device with SnO_2 photoanode suffers from a poor power conversion efficiency (less than 1.5 %) because of faster electron-hole recombination, significantly worse dye adsorption and smaller V_{oc} value due to the 300 mV positive shift in its conduction band edge (with reference to the TiO_2 band position), leading to lower open-circuit voltage and smaller short-circuit photocurrent.15 During the past several decades, considerable efforts have been devoted to synthesize of SnO2 photoanodes with varied morphological architectures ranging from zero,[16] one,[17] two,[18] and complex three-dimensional structures.[19] Up till now, various physical and chemical methods are being undertaken to synthesize SnO_2 photoanodes, including core–shell as building blocks through sol–gel,[20] template-assisted fabrication,[21] hydrothermal,[22] and solvothermal growth etc., methods.[23]

For efficient DSSCs device operation, the interaction of charges at interface between metal oxide and electrolyte/hole transporter, as well as with dye is one of crucial aspects.[24] Careful engineering of the interface is needed to minimize electron loss as well as to offer correctly matching energy levels. Deposition of blocking layer that can inhibit electron recombination and enable a higher degree of dye loading can reduce interface problem of metal oxide. This action also shifts the Fermi energy level of host photoanode so that charge transportation can be easier and faster.[25] Metal oxides like MgO, ZrO_2, Al_2O_3 and SiO_2 etc., have envisaged for this purpose.[26-29] Moreover, high isoelectric point of La_2O_3 enhance dye adsorption on/in-to SnO_2 photoanode surface. Herein, we present a facile spin coated La_2O_3 blocking layer to overcome interface problem of SnO_2 photoanode. The application of La_2O_3 as electron blocking layer has improved charge collection efficiency by reducing number of charge carriers lost *via* recombination.[30] Lanthanide ions (La^{3+}) are known for their ability to form complexes resulted from the co-ordination bonding between f-orbitals of lanthanides and lone electron pairs of various Lewis bases (e.g., acids, amines, aldehydes, alcohols, thiols, etc.).[31,32] Here, La^{3+} ions were

successfully incorporated in/on-to a SnO_2 structure for improving the adsorption of dye molecule, shifting of conduction band position and reducing surface defects. Therefore, surface modification of the SnO_2 photoanodes would be an ideal strategy to improve DSSCs performance.

In this article we propose a simple modification method, which can superimpose a compact La_2O_3 blocking layer as an efficient photoelectron transport fabricated with SnO_2 paste. We expect such a new structural configuration will be able to collectively tackle the electron leakage and low electron transport efficiency problems. Improved charge transfer rate and higher power conversion efficiency are anticipated because of widened electron pathways and reduce the scattering of free electrons among inter-particles. The SnO_2-La_2O_3 photoanode exhibited a higher open-circuit photovoltage (V_{oc}), superior short-circuit current density (J_{sc}), prolonged electron lifetime (τ_η)) and increased dye loading amount in comparison with SnO_2 photoanode. The overall power efficiency (η %) of the La_2O_3-SnO_2 photoanode is about twice compared to SnO_2 photoanode.

2. Experimental details

All chemicals used as reactants were of analytical grade, and used without any further purification. The SnO_2 photoanode were prepared by using a simple hydrothermal method with firstly using fructose as oxidizing agent and $SnCl_4$ (source for Sn^{4+} ions) *via* chemically induced self-assembly. In a standard experiment procedure, 2.80 g of $SnCl_4.5H_2O$ (Sigma Aldrich, 99.9%) and 1.44 g of fructose (Sigma Aldrich, 99%) were mixed in 80 mL distilled water (Milli-Q water; 18.2 MΩ cm). The mixture was kept for 30 min under constant stirring and then transferred into a 100 mL Teflon lined stainless-steel autoclave. The autoclave was sealed and maintained at 190 °C for 24 h. On completion of reaction, the autoclave was cooled naturally to room temperature (27 °C). The resulting black ($Sn(OH)_2$), could be due to excess Sn^{4+} ions, product was centrifuged at 8000 rpm for 10 min and washed several times with distilled water and ethanol to remove unexfoliated compound. The product was heated in air at 600 °C for 2 h so as to form white powder of SnO_2 containing spherical nanocrystallites. For making viscous slurry, SnO_2 powder 1.0 g was mixed in 8.0 mL ethanol, 0.2 mL acetic acid, 4.5 g α-terpineol, and 0.5 g ethyl cellulose, and stirred for 6 h to form uniform and homogenous slurry. After sonication of SnO_2 slurry for 90 min in an ultrasonic bath SnO_2 photoanodes were obtained by using doctor-blade method onto FTO substrate (15 Ω, TEC 8, Pilkington glass). Finally, these photoanodes of SnO_2 were heat treated at 450°C for 1 h so as to evaporate solvents and to get compact SnO_2 photoanodes.

Furthermore, deposition of La_2O_3 blocking layers were carried out on SnO_2 photoanode by using spin-coating method. 0.05 M lanthanum nitrate was dissolved in an isopropanol solution and allowed to fix on SnO_2 substrates under 2000 rpm for 60 s. We also tried it at higher/lower spin rate but performance on either side was decreased. On lowing spin rate performance was poor due to formation of thick La_2O_3 insulating layer that was not allowing to pass excited electrons to SnO_2. Therefore, all photoelectrons might follow reverse path with major recombination possibility. On the other hand, on increasing spin rate could produce extremely thin La_2O_3 layer through which quantum confinement could have limitation to pass all photoelectrons across and thereby few photoelectrons might traverse in reverse direction by reducing performance. In this case, the DSSCs performance of 2000 rpm was superior to that of SnO_2 photoanode indicating an importance of thin layer on photoanode. The spin-coated SnO_2-La_2O_3 photoanodes were heat-treated at 450°C for 30 min. After adding La_2O_3 layers there was no obious difference in average thickness i.e. 20 micron of SnO_2 (see Fig. S1of Supporting Information (SI)). After annealing both i.e. SnO_2 and SnO_2-La_2O_3 electrodes were immersed into 0.03 mM N719 dye solution (ethanol + acetonitrile) for 24 h to adsorb dye molecule. Surface digital photoimages of SnO_2 and SnO_2-La_2O_3 photoanodes were obtained from field-emission scanning electron microscopy (FE-SEM, Nova nano SEM200-FEI). The high-resolution transmission electron microscopy (HR-TEM) and selected area electron diffraction (SAED) measurements were performed using a FEI TECNAI G2 S-TWIN equipped with a LaB6 cathode and a GATAN MS794 P CCD camera. The micrographs were obtained at an acceleration voltage of 200 kV. The SnO_2 and SnO_2-La_2O_3 photoanodes were separated from substrate with a scalpel blade. The powders collected were suspended in ethanol separately and dropped onto a Formvar/carbon, 200 mesh TH, copper grids before HR-TEM measurements. The structural change, if there is any, of SnO_2 and SnO_2-La_2O_3 photoanodes were confirmed from the X-ray diffraction (XRD) spectra (XRD-6000, Shimadzu, Japan) obtained with Cu-Kα radiations (λ= 0.1542 nm). Diffraction patterns were recorded from 20° to 80° along 2θ with a 2° min^{-1} scan-speed. For X-ray photoelectron spectroscopy (XPS), a surface-sensitive quantitative spectroscopic technique, spectra of the photoanodes were acquired with PHI 5000 VersaProbe (Ulvac-PHI) under high vacuum conditions (6.8 x 10-8 pa) using a monochromatic Al Kα X-ray source (1486.6 eV). The data were collected from a spot size of 100 x 100 μm^2. The carbon 1s peak (284.6 eV) was used for internal calibration as a reference. UV-Vis absorption spectra were recorded using a Varian Cary 5000 spectrophotometer instrument. The amounts of dye molecules adsorbed onto SnO_2 and SnO_2-La_2O_3 photoanodes were obtained by dipping them in 0.1 M NaOH solution (ethanol and water at 50:50 ratio by volume) for 24 h at room temperature to desorb attached dye molecules. Volume of solutions was kept constant at 5 mL for dye desorption. The photoanodes, free from the back mask, with each of 0.25 cm^2 area were illuminated from the FTO side with simulated sunlight from a 150 W xenon lamp (Sun 2000 solar simulator, ABET Technologies, USA) equipped with an air-mass filter A.M. 1.5G with a corrected intensity of 1 sun (100 $mWcm^{-2}$) at the photoanode surface. Current density-applied voltage (*J-V*) spectra of SnO_2 and SnO_2-La_2O_3 photoanodes were obtained with the help of a Keithley 2400 source meter. The electrochemical impedance spectroscopy (EIS) and Mott–Schottky analysis measurements were recorded on IviumStat Technologies, Netherland, where the frequency range was varied from 0.1Hz to 100 KHz and Mott–Schottky analysis measurements were measured in 0.1 M Na_2SO_4 electrolyte with a three-electrode configuration. Three electrode system was used platinum plate as a counter electrode, Ag/AgCl as reference electrode, and SnO_2/SnO_2-La_2O_3 as working electrodes i.e. photoanode. The photoluminescent (PL) spectroscopy was measured using Hitachi F-7000 fluorescence spectrophotometer unit. The incident photon-to-current conversion efficiency (IPCE) of both photoanodes were measured using a xenon lamp recorded without bias under illumination with respect to a calibrated Melles-Friot silicon diode and by changing the excitation wavelength (McScience K3100 Spectral IPCE measurement system and Polaronix® K102 Signal Amplifier).

3. Results and discussion

3.1. Surface morphology and structure

The FE-SEM images of SnO_2 and SnO_2-La_2O_3 photoanodes are shown in Fig. 1 (a, b) where there was no obvious difference in surface appearance. Both surfaces were not polished and compact. Few voids were seen in SnO_2-La_2O_3 photoanode. SnO_2 photoanode was composed of agglomerated-type islands with several 40-50 nm spherical crystallites. After La_2O_3 formation SnO_2 nanocrystallites were close to one another and there was no as such gap between them. Both photoanodes were scanned for HR-TEM measurement by assuming there will be a separate La_2O_3 layer in/on-to SnO_2 crystallites. The low magnification HR-TEM images (Figure 1 c, d) show individual nanoparticle. From these images it was difficult to trace out the changes in lattice structure as excepted, but nothing was clearly observed. Continuous sharp circles in SAED (selected area electron diffraction) pattern (insets of Fig. 1 c, d) confirmed polycrystalline nature. Lattice images were clearly observed, indicating that these nanoparticles were having high crystallinity. A lattice spacing of 0.33 nm, consistent to reported result, from (110) plane of SnO_2 was estimated.[33] The EDX analysis (Fig.S2) revealed that both SnO_2 and SnO_2-La_2O_3 photoanodes were composed of Sn, O, and La. The absence of peak correspond to impurity was confirming the formation of pure and defect-free SnO_2. Fig. S2 (b) presents La and O peaks which certainly were from the La_2O_3 blocking layer in/on-to SnO_2 photoanode, confirming quantitatively the presence of La_2O_3 in/on-to SnO_2, which otherwise was failure from TEM and XRD measurements (see later). The XRD pattern (Figure 1 e) of SnO_2 photoanode demonstrated most of the Bragg reflection peaks were from tetragonal phase with lattice constants, a =4.7382 Å, and c =3.1871 Å (JCPDS No. 41-1445).

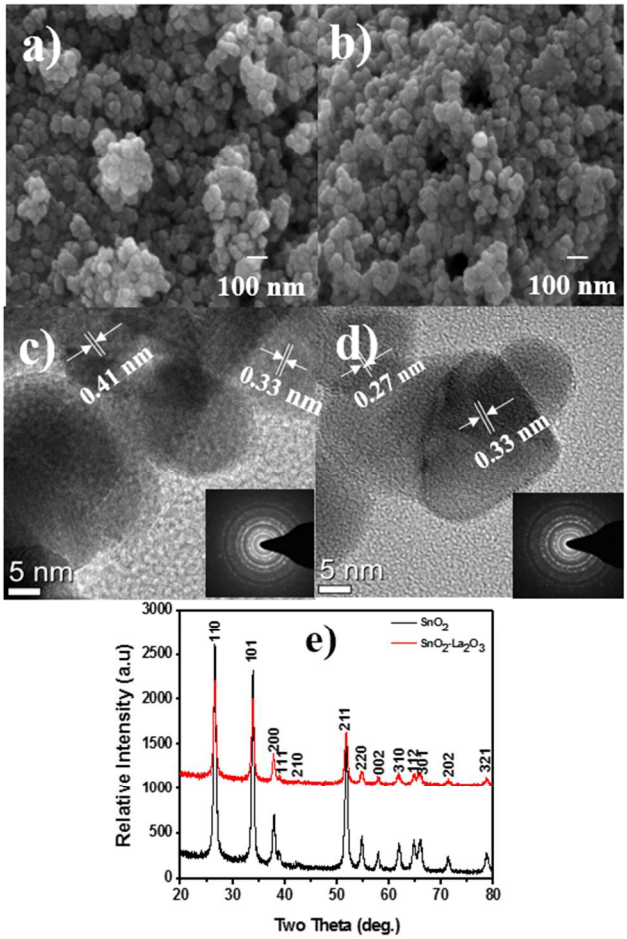

Fig. 1 FE-SEM images of; a) SnO_2 and b) SnO_2-La_2O_3. TEM images of; c) SnO_2 and d) SnO_2-La_2O_3, and e) XRD patterns of SnO_2 and SnO_2-La_2O_3 (powders scratched from respective substrates).

After SnO_2-La_2O_3 photoanode, due to extremely thin layer of La_2O_3 there was no conspicuous lattice distortion of XRD pattern indicating that thin La_2O_3 might either have covered empty spaces or formed a thin layer on SnO_2 spherical nanoparticles.

3.2. Optical, *J-V* and surface area studies

Fig. 2a shows UV-vis absorption spectra for dye-absorbed SnO_2 and SnO_2-La_2O_3 photoanodes, where in later case due to increased dye molecules substantially high absorbance compared to SnO_2 was obtained. Dye amounts over SnO_2 and SnO_2-La_2O_3 photoanodes, estimated from the Uv-Vis spectrams were 0.68×10^{-7} and 1.23×10^{-7} mol cm^{-2}, respectively. The higher number of dye molecules onto SnO_2-La_2O_3 photoanode compared with SnO_2 was due to higher basicity of La_2O_3. If the blocking layer materials are more basic than SnO_2, the carboxyl groups in N719 dye molecules are more easily adsorbed to surface of coating layers.[34] The ~10.0 isoelectric point[35] of La_2O_3 was considerably greater than that of SnO_2 (~5.5).[36] This means that the surface of SnO_2-La_2O_3 photoanode was more basic than that of SnO_2, leading to a significant improvement in dye absorption. Fig. S3 illustrates *J-V* behaviors of SnO_2-La_2O_3 photoanodes under dark where in all electrodes dark current density was lower than La_2O_3 embedded SnO_2 electrodes (for simplicity we also measured dark and light J-V performances of SnO_2 electrode for various layers of La_2O_3 i.e. 2, 4, 6 and 8 spin-coating numbers was shown Fig.S3 and S4). Forward-biased dark current density in SnO_2 photoanode, a result of an electrochemical reaction that involves the redox couple, was higher than that SnO_2-La_2O_3 photoanodes, indicating highest leakage current in the SnO_2 photoanode on account of its higher charge-transfer resistance across the electrode/electrolyte interface compared to SnO_2-La_2O_3 photoanodes. Dark current density was higher initially for SnO_2 photoanode surface and slowly reduced when La_2O_3 blocking layer was in/on-to SnO_2 photoanode. Excess charge leakage from SnO_2 photoanode might favour higher dark current density which decreased with SnO_2-La_2O_3 photoanode due to the increase in the La^{2+}/dye complex layer thickness by preventing the charge carrier transport ion. Fig. 2b shows the *J-V* measurements of SnO_2 and SnO_2-La_2O_3 (under 1 spin coating as performance of 2 was less, see Fig. 2 (b) and Table S1 for more details) photoanodes, whose detailed photovoltaic parameters are listed in Table 1. Among all SnO_2-La_2O_3 electrodes, DSSCs performance of SnO_2-La_2O_3 photoanodes obtained for 1 spin-coating layer was superior to that of SnO_2 and 2, 4, 6 and 8 layers, signifying an importance of encapsulation in DSSCs. It is noteworthy that the performance of all La_2O_3 encapsulated SnO_2 was higher than SnO_2.

Table 1: DSSCs parameters for SnO_2 and SnO_2-La_2O_3 photoanodes obtained from *J-V* measurements.

Photoanode	Dye adsorption x10^{-7}mol cm^{-2}	J_{sc} (mA cm^{-2})	V_{oc} (V)	FF	η (%)
SnO_2	0.68	8.30	0.40	0.49	1.66
SnO_2- La_2O_3	1.23	13.70	0.46	0.48	3.1

SnO_2 electrode showed poor DSSCs performance with V_{oc} of 0.40V, J_{sc} of 8.30 $mAcm^{-2}$, *FF* of 0.49, and power conversion efficiency of 1.61%. Lower V_{oc} of 0.40 V was due to the more positive conduction band edge of SnO_2.[37] SnO_2-La_2O_3 photoanode revealed two-fold improvement in DSSCs parameters

compare to SnO_2 photoanode. V_{oc} was increased to 0.55V from 0.40 V, J_{sc} to 10.35 from 8.30 mA cm^{-2}, *FF* to 52 from 49% and efficiency to 3.0 from 1.61%. Improvement in V_{oc} was due to an increase in the conduction band level to more negative side after surface modification of SnO_2 by La_2O_3 layer. Enhancement in J_{sc} was attributed to excess; a) dye amount (in Fig. 2a), b) active surface area, c) iso-electric point and slower recombination rate of electrons due to La_2O_3 layer.[38] Furthermore, the electron recombination in DSSC can be characterized by open-circuit voltage decay (OCVD) measurement. This measurement was conducted when a steady state V_{oc} of DSSCs was obtained under the solar light illumination and decay of V_{oc} was monitored when illumination was stopped. It is well-established that V_{oc} is highly dependent on the quasi-Fermi level, i.e., the electron density at conduction band of photoanode.[39]

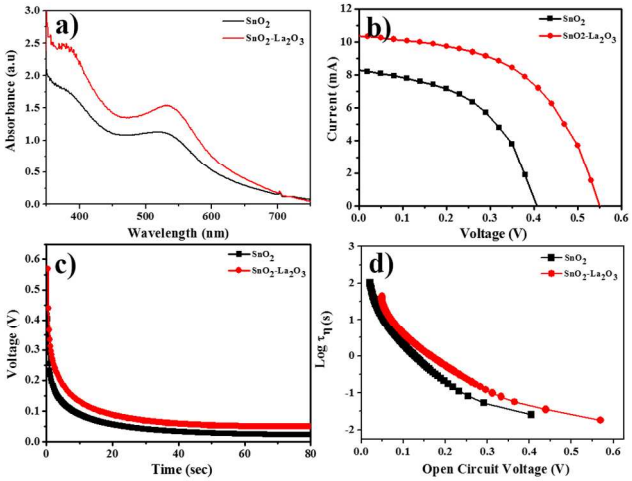

Fig. 2 a) UV-Vis, b) J-V, c) OCVD, and d) log τ_η vs.V_{oc} of SnO_2 and SnO_2-La_2O_3 photoanodes.

Therefore, the decay of V_{oc} can be used to reflect regression of electron density in conduction band of photoanode. OCVD measurement has been widely used as a kinetic parameter, which contains useful information on rate constant of electron transfer process in DSSCs. The electron lifetime (τ_η) was calculated by fitting the photovoltage decay plot obtained from the OCVD measurement and applying an equation developed by Bisquert *et al.*[40] The longer electron lifetime in SnO_2-La_2O_3 photoanode implied a lower charge recombination rate; improved electron transfer efficiency.[41] Moreover, La_2O_3 blocking layer on SnO_2 photoanode might improve interparticles connection due to which efficient transfer of electrons into conduction band to external circuit through shortest pathway could be plausible. The shortest pathway for electron transfer, either help to reduces electron recombination or considerably boosts the transfer velocity of electron.[42] Therefore, the electron lifetime of SnO_2-La_2O_3 photoanode was significantly extended (Fig. 2 c, d) compared with SnO_2 photoanode. The Brunauer-Emmett-Teller (BET) surface area and pore-diameter (not shown) of SnO_2 photoanode were 12.19 $m^2.g^{-1}$ and 31.11 nm while for SnO_2-La_2O_3 photoanode respective parameters were 12.84 $m^2.g^{-1}$ and 27.67 nm. The high surface area and less pore-diameter of SnO_2-La_2O_3 photoanode were responsible for adsorbing excess dye molecules[43] compared to SnO_2 photoanode

3.3. Surface analysis

The XPS measurement was used to examine chemical states and surface composition of SnO_2 and SnO_2-La_2O_3 photoanodes to corroborate results of EDX analysis (Fig. 3a-c). In XPS spectrum of SnO_2 shows (Fig. 3a) Sn, O, and C peaks. The Fig. 3b is XPS survey spectrum after La_2O_3 layering, where Sn, La, O, and C peaks were detected and there was no any trace of others.

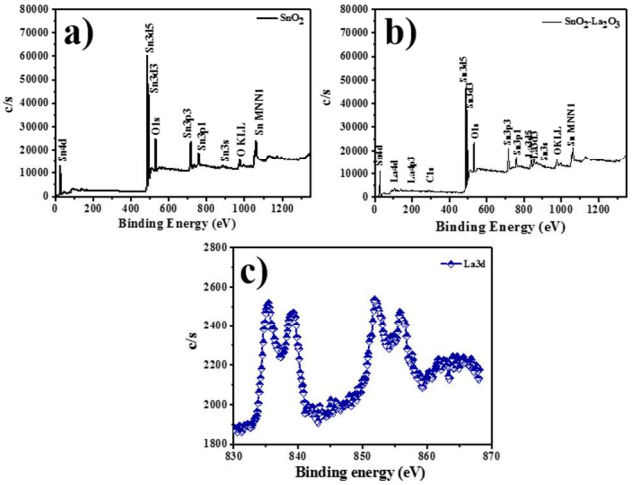

Fig. 3 XPS plots for; a) SnO_2, b) SnO_2-La_2O_3, and c) La3d of SnO_2-La_2O_3.

The new peak of La was detected in XPS indicating the presence of La_2O_3 layer on SnO_2 photoanode. The carbon peak at 284.8 eV was assigned which could be due to residual carbon in sample and hydrocarbons from the XPS instrument itself. In Figure 3c i.e. SnO_2-La_2O_3 photoanode the binding energy peaks were obtained at 834.8 eV, 840.4 eV, 851.8 eV, and 856.4eV which were caused by 3d states of La element, supporting qualitatively existence of La_2O_3 in/on-to SnO_2.[44]

3.4. Charge transport kinetics

To further understand the interfacial charge transfer kinetics, in Figure 4a we performed EIS measurements of SnO_2 and SnO_2-La_2O_3 photoanodes. The EIS spectra for these two photoanodes were measured from 0.1Hz to 100 KHz. Clearly two semicircles were visible for both devices. Semicircle on the left hand side (high frequency region) was due to charge transfer resistance (R_1) between counter electrode and electrolyte and right hand side (low frequency region) was assigned to charge transfer resistance (R_2) in photoanode.[45,46] The size of second semicircle (the value of R_2) was an important factor affecting the photovoltaic parameter. The SnO_2-La_2O_3 electrode exhibited 33.11Ω R_2 value which was considerably smaller than that of SnO_2 (38.85Ω) indicating the faster electron generation and transportation as well as lower hole-electron recombination rate in former case than in later. The La_2O_3 layer tightly hold spherical SnO_2 nanocrystallites permitting electron transportation over a longer distance with less diffusive hindrance.[47,48] The electrochemical parameters obtained from Nyquist plots for both electrodes are summarized in Table 2.

Table 2: Obtained electrochemical parameters for SnO_2 and SnO_2-La_2O_3 electrodes.

Photoanode	R_S (Ω cm^2)	R_1 (Ω cm^2)	R_2 (Ω cm^2)
SnO_2	9.89	3.18	39.27
SnO_2-4L La_2O_3	8.37	5.78	30.77

Fig. 4b compares the IPCE spectra of SnO_2 and SnO_2-La_2O_3 photoanodes. The SnO_2 photoanode presented relatively lower IPCE with maximum value of ~53% which could be due to less number of dye molecules adsorbed and higher recombination rate.

In addition, the SnO_2-La_2O_3 photoanode demonstrated as high as ~60% IPCE at 530 nm. Increase in IPCE was due to; a) excess dye molecules, b) reduction in electron recombination, and c) enhanced light scattering ability.[49]

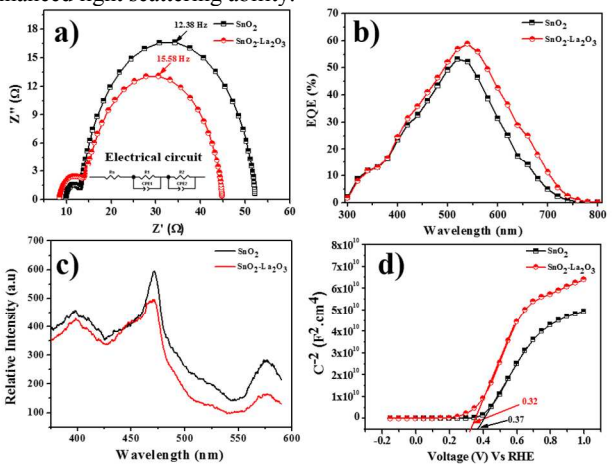

Fig 4. a) EIS, b) IPCE, c) PL, and d) Mott-Schottkey measurements of SnO_2 and SnO_2-La_2O_3 electrodes

The room temperature PL spectra of the SnO_2 and SnO_2-La_2O_3 photoanodes are shown in Fig. 4c. Here, the spectra were normalized by UV emission peak at 350 nm. It was noted that the peak intensity of visible emission of SnO_2-La_2O_3 was much weaker compared to SnO_2. We presumed that the formation of a La_2O_3 layer on SnO_2 might reduce surface defects and minimize recombinations at an interface.[50] Fig. 4d shows Mott-schottky plots for SnO_2 and SnO_2-La_2O_3 photoanodes measured in 0.1 M Na_2SO_4 aqueous electrolyte to determine respective flat band potentials (E_{fb}). The E_{fb} of photoanode is very important parameters because V_{oc} is closely related to difference between the red-ox potential in electrolyte and Fermi level of a semiconductor. In this plot a negative shift of E_{fb} means a shift away from the red-ox potential, thereby an increase of V_{oc}. The calculated E_{fb} values of SnO_2 and SnO_2-La_2O_3 photoanodes were 0.37 and 0.32 V (*vs.* Ag/AgCl), respectively. Bandara *et al.* reported MgO surface modified SnO_2 photoanode with a negative shift of E_{fb} due to the basic surface properties.[51] Basic character of MgO (isoelectric point ~12) produces a deprotonation and interfacial dipole on the SnO_2 surface and that causes negative shift of E_{fb}. In our case La_2O_3 show basic characteristics (isoelectric point ~10.5). The basic property of La_2O_3 might cause negative shift in E_{fb} in the present case, counteracting the effect of lower-lying conduction band position of SnO_2.[52]

The cathodic polarization Tofel curves recorded for SnO_2 and SnO_2-La_2O_3 photoanodes in the dark are shown in Figure 5. The difference in behaviour of the curves can be ascribed to a different charge-transfer processes at photoanode interface.[53] With negative bias applied to a semiconductor electrode, charge will first fill the empty surface states below the conduction band edge and then become accumulated in the space charge layer. A marked increase in cathodic current will occur when the potential exceeds the flat band edge in the negative scan direction.[54] The difference in cathodic polarization behaviours indicated that the flat-band edge of SnO_2-La_2O_3 shift negatively as compared with SnO_2 photoanode; consistent to earlier Mott–Schottky measurement (Figure 4 d).

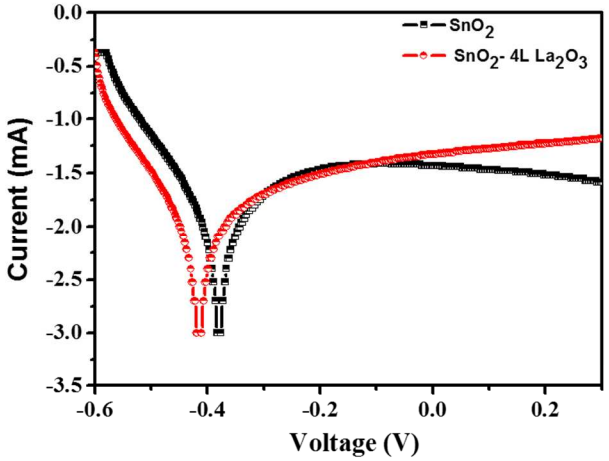

Fig 5. Cathodic polarization Tofel measurements for SnO_2 and SnO_2-La_2O_3 electrodes in 0.5 M Na_2SO_4 electrolyte. Plot graph from -0.5 to 0.0

4. Conclusions

In summary, we have synthesized SnO_2 and SnO_2-La_2O_3 photoanodes using two step processes *viz.* hydrothermal and spin-coating. Effect of La_2O_3 layering on structure, morphology, surface state and binding energies of SnO_2 was investigated. The presence of La_2O_3 on SnO_2 was quantitatively studied from energy dispersive X-ray analysis and X-ray photoelectron spectroscopy measurements. Dye absorbance in/on-to SnO_2 electrode was increased in the presence of La_2O_3. Both SnO_2 and SnO_2-La_2O_3 photoanodes were loaded with N719 dye for 24 h and changes in DSSCs properties (J-V, OCVD, IPCE and EIS) were monitored. Due to increased optical density caused by an excess dye molecules and reduced charge transfer resistance, remarkable two-fold improvement in power conversion efficiency (3.0%) was obtained for SnO_2-La_2O_3 electrode compared with SnO_2 photoanode (1.6%). The PL spectra proved decrease in peak intensity of SnO_2-La_2O_3, suggesting reduced number of surface states. Moreover, Mott-Schottky analysis of SnO_2-La_2O_3 photoanode showed negative shift in flat band potential, suggesting enhanced electron density and charge transportation rate of photoelectrons towards FTO substrate.

Acknowledgments
The authors acknowledge the support from the Korea Institute of Science and Technology (KIST) institutional program.

[a]*Clean Energy Research Center, Korea Institute of Science and Technology, Seoul, Korea.E-mail: joocat@kist.re.kr; Fax: +8202958-5215; Tel: +82-2958-5217*
[b]*School of Science, Korea University of Science and Technology, 52 Eoeun dong, Yuseong-gu, Daejeon 305-333, Republic of Korea.*

† **Notes and references**

1. M. Gratzel, *Inorganic Chemistry*, 2005, **44**, 6841.
2. Q. Zhang, X. Liu, *small* 2012**, 8,** 3711.
3. S. F. Shaikh, G. Rahman, R. S. Mane, O. S. Joo *Electrochim. Acta,* 2013,**111,** 593.
4. B. E. Hardin, H. J. Snaith, M. D. McGehee, *Nat Photon*, 2012, **6,** 162.
5. M. Gratzel, J. Photochem. Photobio. A: Chem., 2004, **164**, 3.

6. F. Sauvage, D. Chen, P. Comte, F. Huang, L. P. Heiniger, Y. B. Cheng, R. A. Caruso, M. Gratzel, *ACS Nano*, 2010, **4**, 4420-4425.
7. H. Tantang, A. K. K. Kyaw, Y. Zhao, M. B. C. Park, A. I. Y. Tok, Zheng Hu, L. J. Li, X. W. Sun, Q. Zhang, *Chem. Asian J.* 2012, 7, 541.
8. E. Hendry, M. Koeberg, B. O'Regan, M. Bonn, *Nano Lett*., 2006, **6,**755.
9. M. Law, L. E. Greene, J. C. Johnson, R. Saykally, P. Yang, *Nat Mater,* 2005, **4,** 455.
10. X. Dou, N. Mathews, Q. Wang, S. S. Pramana, Y. M. Lam, S. Mhaisalkar, *Nanoscale*, 2011, **3**, 4640.
11. S. F. Shaikh, S. S. Kalanur, R. S. Mane, O. S. Joo, *Dalton Trans.,* 2013, **42,** 10085.
12. K. Sayama, H. Sugihara, H. Arakawa, *Chem. Mater.,* 1998, **10,** 3825.
13. X. Dou, D. Sabba, N. Mathews, L. H. Wong, Y. M. Lam, S Mhaisalkar, *Chem. Mater*. 2011, **23**, 3938.
14. H. Niu, S. Zhang, R. Wang, Z. Guo, X. Shang, W. Gan, S. Qin, L. Wan, J. Xu, *J. Phys. Chem. C*, 2014, **118**, 3504.
15. G. Shang, J. Wu, S. Tang, L. Liu, X. Zhang, *J. Phys. Chem. C*, 2013, **117**, 4345.
16. X. Xu, J. Zhuang, X. Wang, *J. A. Chem. Soc.* 2008, **130** 12527.
17. C. Wang, Y. Zhou, M. Ge, X. Xu, Z. Zhang, J. Z. Jiang, *J. A.Chem. Soc.,* 2009, **132,** 46.
18. B. Wang, Y. H. Yang, C. X. Wang, G. W. Yang, *Chem. Phys. Lett*. 2005, **407,** 347.
19. W. H. Wen, C. F. Ting, M. K. Hung, C. H. Chiou, Y. L. Liu, Z. Liu, K. R. Ratinac, S. P. Ringer, *Nanotech.* 2009, **20,** 055601.
20. Z. Liu, C. Liu, J. Ya, E. Lei, *Renewable Energy,* 2011, **36** 1177.
21. J. Ye, H. Zhang, R. Yang, X. Li, L. Qi, *Small,* 2010, **6** 296.
22. X. Dou, R. R. Prabhakar, N. Mathews, Y. M. Lam, S. Mhaisalkar, *J. Electrochem. Soc.*, 2012,159 (9), H735.
23. G. Cheng, K. Wu, P. Zhao, Y. Cheng, X. He, K. Huang, *J. of Cryst. Growth*, 2007, **309**, 53.
24. A. N. M. Green, E. Palomares, S. A. Haque, J. M. Kroon, J. R. Durrant, J. *Phys. Chem. B*, 2005, **109**, 12525.
25. S. F. Shaikh, R. S. Mane, O. S. Joo, *RSC Adv.*, 2014, **4** 35919.
26. P. Docampo, P. Tiwana, N. Sakai, H. Miura, L. Herz, T. Murakami, H. J. Snaith*, J. Phys. Chem. C*, 2012, **116**, 22840.
27. E. Palomares, J. N. Clifford, S. A. Haque, T. Lutz, J. R. Durrant, *J. Am. Chem. Soc.,* 2002, **125**, 475.
28. C. Prasittichai, J. T. Hupp, *J. Phy. Chem. Lett.,* 2010, **1,** 1611.
29. S. Son, S. H. Hwang, C. Kim, J. Y. Yun, J. Jang, *ACS App. Mate. & Inter.*, 2013, **5**, 4815.
30. H. Yu, B. Xue, P. Liu, J. Qiu, W. Wen, S. Zhang, H. Zhao, *ACS App. Mate. & Inter.*, 2012, **4**, 1289
31. Y. Zhang, H. Xu, Y. Xu, H. Zhang, Y. Wang, *J. Photoche. Photobio. A: Chem.*, 2005, **170,** 279.
32. S. Zhang, Z. Zheng, J. Wang, J. Chen, *Chemosphere*, 2006, **65,** 2282.
33. G. Feng, W. Shufen, C. Hongming, L. Chunzhong, *Nanotech.,* 2008,19, 095708.
34. A. Kay, M. Graetzel, *Chem. Mater.,* 2002, **14**, 2930.
35. K.Y. Kim, Y. H. Yun, *J. Ceram.Proce. Research*, 2007, **8,** 421.
36. E. Ramasamy, J. Lee, Energy Environ. Sci., 2011, **4**, 2529.
37. S. Gubbala, V. Chakrapani, V. Kumar, M. K. Sunkara, *Adv. Func.Mater.*, 2008, **18**, 2411.
38. J. Qian, P. Liu, Y. Xiao, Y. Jiang, Y. Cao, X. Ai, H. Yang, *Adv. Mater.,* 2009, **21**, 3663.
39. C. Y. Chen, M. Wang, J. Y. Li, N. Pootrakulchote, L. Alibabaei, C.H Ngoc-le, J. D. Decoppet, J. H. Tsai, C. Graetzel, C. G. Wu, S. M. Zakeeruddin, M. Gratzel, *ACS Nano,* 2009, **3**, 3103.
40. J. Bisquert, A. Zaban, M. Greenshtein, I. Mora-Sero, *J. Am. Chem.Soc.,* 2004, **126,** 13550.
41. E. Ghadiri, N. Taghavinia, S.M. Zakeeruddin, M. Graetzel, J. E. Moser, *Nano Lett.,* 2010, **10,** 1632.
42. H. Yu, S. Zhang, H. Zhao, B. Xue, P. Liu, G. Will, *J. Phys. Chem. C,* 2009, **113**, 16277.
43. M. Adachi, Y. Murata, J. Takao, J. Jiu, M. Sakamoto, F. Wang, *J Am.Chem. Soc.,* 2004, **126,** 14943.
44. H. Wong, H. Iwai, K. Kakushima, B. L. Yang, P. K. Chu, *J. Electroche. Soc.,* 2010, **157**, G49.
45. R. S. Mane, D. V. Shinde, S. Joon Yoon, S. B. Ambade, J. Kee Lee, S. H. Han, *Appl. Phys. Lett.,* 2012, **101**, 033906.
46. A. K. K. Kyaw, H. Tantang, T. Wu, L. Ke, C. Peh, Z. H. Huang, X. T. Zeng, H. V. Demir, Q. Zhang, and X. W. Sun, *Appl. Phys. Lett*. 2006, **89**, 253512.
47. D.V. Shinde, D. Y. Ahn, V. V. Jadhav, D. Y. Lee, N. K. Shrestha, J. K. Lee, H.Y. Lee, R. S. Mane, S. H. Han, *J. Mater. Chem. A,* 2014, **2**, 5490.
48. A. K. K. Kyaw, H. Tantang, T. Wu, L. Ke, J. Wei, H. V. Demir, Q. Zhang, X. W. Sun*, J. Phys. D: Appl. Phys*., 2012, 45, 165103.
49. A. Allegrucci, N.A. Lewcenko, A.J. Mozer, L. Dennany, P. Wagner, D.L. Officer, K. Sunahara, S. Mori, L. Spiccia, *Energy Environ. Sci.,* 2009, **2**, 1069.
50. J. Chung, J. Myoung, S Oh, S. Lim, *J. Phys. Chem. C*, 2010, **114,** 21360.
51. J. Bandara, C. M. Divarathne, S. D. Nanayakkara, *Sol. Energy Mater. Solar Cells,* 2004, **81** , 429.
52. M H. Kim, Y. U. Kwon, *J. Phys. Chem. C,* 2009, **113,** 17176.
53. X. Feng, K. Shankar, M. Paulose, C. A. Grimes, *Angew. Chem.* 2009, **121**, 8239.
54. F. Fabregat-Santiago, E. M. Barea, J. Bisquert, G. K. Mor, K. Shankar, C. A. Grimes, *J. Am. Chem. Soc.* 2008, **130**, 11312 .